Perturbative analytical solutions of the magnetic forward problem for realistic volume conductors

Guido Nolte[a)]
Neurophysics Group, Department of Neurology, Klinikum Benjamin Franklin Freie Universität Berlin, Hindenburgdamm 30, D-12200 Berlin, Germany

Thomas Fieseler
Institute of Medicine, Research Center Jülich, D-52425 Jülich, Germany

Gabriel Curio
Neurophysics Group, Department of Neurology, Klinikum Benjamin Franklin Freie Universität Berlin, Hindenburgdamm 30, D-12200 Berlin, Germany

(Received 23 March 2000; accepted for publication 8 November 2000)

The magnetic field induced by a current dipole situated in a realistic volume conductor cannot be computed exactly. Here, we derive approximate analytical solutions based on the fact that in magnetoencephalography the deviation of the volume conductor (i.e., the head) from a spherical approximation is small. We present an explicit integral form which allows to calculate the *n*th order Taylor expansion of the magnetic field with respect to this deviation from the corresponding solution of the electric problem of order $n-1$. Especially, for a first order solution of the magnetic problem only the well-known electric solution for a spherical volume conductor is needed. The evaluation of this integral by a series of spherical harmonics results in a fast algorithm for the computation of the external magnetic field which is an excellent approximation of the true field for smooth volume conductor deformations of realistic magnitude. Since the approximation of the magnetic field is exactly curl-free it is equally good for all components. We estimate the performance for a realistic magnitude of deformations by comparing the results to the exact solution for a prolate spheroid. We found a relevant improvement over corresponding solutions given by the boundary element method for superficial sources while the performance is in the same order for deep sources. © *2001 American Institute of Physics.* [DOI: 10.1063/1.1337089]

I. INTRODUCTION

Current source reconstructions from magnetoencephalographic[1] (MEG) measurements crucially depend on the accuracy of the forward solution, i.e., the calculation of the magnetic field due to a dipole placed in a volume conductor. Exact analytical solutions both of the electric and magnetic forward problem are only known for special volume conductors[2–10] with the sphere being the most prominent.[3] These special volume conductors are in general an insufficient approximation of the inner boundary of the scull, the most relevant part of the whole volume conductor, the head.

So far, solutions for complex geometries can only be obtained by numerical methods solving the differential or the integral form of the corresponding Maxwell equations by means of the ''finite element method'' (FEM)[11] or the ''boundary element method'' (BEM),[12–14] respectively. While both methods are applicable for a large class of volume conductors they are very time consuming and require a large amount of disk space. Furthermore, originally analytical operations like differentiation[15–18] might lead to large errors if applied on solutions given only numerically. While in BEM this drawback can in principle be avoided it is inherent in FEM.

Here, we propose a new method based on the fact that for MEG deviations of the realistic volume conductor from the spherical approximation are small. The magnetic field can therefore formally be expressed as a spherical solution plus a correction. While the functional dependence of this correction on the deviation from the sphere can, of course, not be solved exactly, we will derive an equation to exactly compute the low order Taylor expansion of this functional. Remarkably, it will turn out that for a first order Taylor expansion the corresponding solution of the electric problem[19] is not needed, and the solution for the magnetic field can be expressed as a surprisingly simple integral with no unknown variables left.

For an explicit evaluation of this integral we have to express the source, the solution, and the deformation of the sphere in finite series of spherical harmonics.[19,20] The latter implies that though there is no principal limit in the complexity of the volume conductor there will be a practical one depending on the specific computer implementation of the algorithms. In this sense we make two assumptions on the volume conductor: (a) the deformation of the sphere is small compared to its radius, and (b) the deformation is smooth, i.e., sufficiently fittable by the number of chosen surface parameters. For MEG, both conditions are matched, in particular for cortical sources where the upper hemisphere is the relevant part of the volume conductor.

This article is organized as follows. In Sec. II A we recall the formal expressions for the magnetic field and the parameterization of the volume conductor. The fundamental

a)Electronic mail: nolte@CS.unm.edu

equation of this article is derived in Sec. II B where the radial component of the magnetic field is expressed as a simple integral. Based on this equation we present in Sec. II C the algorithm to compute the magnetic fields in arbitrary direction. In Sec. III we present fundamental properties of the forward calculation, namely convergence, the dependence of the magnetic field on the spatial frequencies of the deformed volume conductor, and computational cost. In Sec. IV we make detailed comparisons of the perturbative, spherical, and BEM solutions for a prolate spheroid, and we finally discuss our results in Sec. V.

Let us make a final remark: we do not present calculations for realistic volume conductors found from magnetic resonance imaging which is beyond the scope of this article. Furthermore, since the accuracy of BEM solutions themselves *crucially* depends on dipole depth, direction, and the component of the calculated magnetic field, there is no rigorous way to judge the two different solutions.

II. THEORY

A. Backgorund

Brain activity is quite generally described by a stationary, primary current $\mathbf{J}^P(\mathbf{r})$. The primary current induces a ''return'' or ''volume'' current $\mathbf{J}^V(\mathbf{r})$ which together with $\mathbf{J}^P(\mathbf{r})$ makes up the total current $\mathbf{J}(\mathbf{r})=\mathbf{J}^P(\mathbf{r})+\mathbf{J}^V(\mathbf{r})$. In contrast to the active part $\mathbf{J}^P(\mathbf{r})$, which can be arbitrary, the volume current is assumed to be induced by an electric field within a medium[3]

$$\mathbf{J}^V=\sigma(\mathbf{r})\mathbf{E}=-\sigma(\mathbf{r})\nabla V(\mathbf{r}), \tag{1}$$

where $V(\mathbf{r})$ is the electric potential at point $\mathbf{r}$ and $\sigma(\mathbf{r})$ is the conductivity. Stationarity implies that the total current must have vanishing divergence

$$\nabla[\mathbf{J}^P(\mathbf{r})-\sigma(\mathbf{r})\nabla V(\mathbf{r})]=0, \tag{2}$$

which completely determines $\mathbf{J}$ as a function $\mathbf{J}^P(\mathbf{r})$.

The magnetic field can now formally be calculated from $\mathbf{J}$ using Biot–Savart's law as

$$\mathbf{B}(\mathbf{r}')=-\frac{\mu_0}{4\pi}\int dV\mathbf{J}(\mathbf{r})\times\nabla\frac{1}{|\mathbf{r}'-\mathbf{r}|}. \tag{3}$$

In this article we assume that the conductivity $\sigma(\mathbf{r})$ is homogeneous and isotropic within a volume conductor C with boundary ∂C. This implies that the volume conductor consists of one compartment which is known to be a sufficient approximation for the *magnetic* forward calculation.[21,22] However, generalization of the presented method to more compartments is straightforward and will be briefly discussed later. For one compartment the magnetic field can be expressed as a surface integral by means of Green's theorem[3]

$$\mathbf{B}(\mathbf{r}')=\frac{\mu_0\sigma}{4\pi}\int_{\partial C}d\mathbf{S}\times\frac{\mathbf{r}-\mathbf{r}'}{|\mathbf{r}-\mathbf{r}'|^3}V(\mathbf{r})+\mathbf{B}^{\mathrm{inf}}(\mathbf{r}'), \tag{4}$$

where $\mathbf{B}^{\mathrm{inf}}$ is the magnetic field resulting from the primary part of the current density alone and V is the electric potential on the surface of volume conductor.

In order to find an approximate analytical solution we have to analytically *define* the surface.[19,20] We assume that a function f exists such that the surface is given by the image of a function $\mathbf{G}:[0,\pi]\times[0,2\pi]\rightarrow\mathbb{R}^3$ with

$$\mathbf{G}(\Theta,\Phi)=\begin{bmatrix} r(\Theta,\Phi)\sin\Theta\cos\Phi \\ r(\Theta,\Phi)\sin\Theta\sin\Phi \\ r(\Theta,\Phi)\cos\Theta \end{bmatrix} \tag{5}$$

and

$$r(\Theta,\Phi)=R+f(\Theta,\Phi). \tag{6}$$

R is the unperturbed, constant radius of the spherical approximation of the real volume conductor. For this parameterization of the realistic volume conductor the integral measure $d\mathbf{S}$ can be explicitly expressed as[19]

$$d\mathbf{S}=d\Theta d\Phi r\sin\Theta\left(r\mathbf{e}_R-\frac{\partial f}{\partial\Theta}\mathbf{e}_\Theta-\frac{1}{\sin\Theta}\frac{\partial f}{\partial\Phi}\mathbf{e}_\Phi\right). \tag{7}$$

Here we expand f in the basis of spherical harmonics up to order P

$$f(\Theta,\Phi)=\sum_{p=0}^{P}\sum_{q=-p}^{p}\beta_{pq}Y_{p,q}(\Theta,\Phi) \tag{8}$$

with $\beta_{p-q}=\beta_{pq}^{\star}$ since f is real. We refer to (β_{pq}) as the multipole coefficients of the realistic surface which are regarded as a given input which can be derived from a subject's cranial magnetic resonance imaging. For phase and normalization conventions of the spherical harmonics we refer to Ref. 19.

If the volume conductor is sufficiently smooth we can expect that we only need a few terms in Eq. (8) to describe the head shape with a high accuracy. It was found that an expansion up to order $P=5$ is sufficient to describe details that are as complicated as the neck.[20] Explicit calculations are done here up to $P=6$. Signals of brain activity which can be measured with high signal-to-noise ratio (and, hence, making the consideration of a realistic volume conductor worthwhile) basically originates from in the superficial human cortex close to the upper hemisphere, and we can expect that our expansion provides a sufficient description of the head for this case. In general, the splitting of a volume conductor into a sphere and a deformation is not unique. The most convenient choice depends on the specific volume conductor and the region of interest — if one exists. The dependence of the forward calculation on this very choice will be demonstrated in Sec. IV.

B. Perturbative calculation of the magnetic field

In principle the perturbative calculation of $\mathbf{B}(\mathbf{r}')$ requires the knowledge of the measure $d\mathbf{S}$, the Green's function and the potential V up to the *same* order as $\mathbf{B}$. However, the calculation can be tremendously simplified if one uses the same trick as for the spherical case, i.e., we merely calculate the radial component of $\mathbf{B}$. From this component the total magnetic field is easily found by means of integration in radial direction (yielding the magnetic scalar potential) and finally taking the gradient. The crucial advantage is that the radial part of the measure $d\mathbf{S}$ does not contribute to the radial

component of **B**, but the nonradial part is of order *f*. Thus, an *n*th order calculation of

$$B_{r'} \equiv \mathbf{e}_{r'} \cdot \mathbf{B} \tag{9}$$

requires only the Green's function and V up to order $n-1$. Especially, to calculate **B** up to first order we only need to know the electric potential for a spherically symmetric volume conductor.

For the nonspherical part of the radial component of **B** we explicitly get

$$\begin{aligned} B_{r'} - B_{r'}^{\inf} &= \frac{\mu_0 \sigma}{4\pi} \mathbf{e}_{r'} \int d\Theta d\Phi \sin\Theta r \left(-\frac{\partial f}{\partial \Theta} \mathbf{e}_\Theta - \frac{1}{\sin\Theta} \frac{\partial f}{\partial \Phi} \mathbf{e}_\Phi \right) \times \frac{\mathbf{r}}{|\mathbf{r}-\mathbf{r}'|^3} V(\Theta,\Phi) \\ &= \frac{\mu_0 \sigma}{4\pi} \mathbf{e}_{r'} \int d\Theta d\Phi \sin\Theta \, r \left(\frac{\partial f}{\partial \Theta} \mathbf{e}_\Phi - \frac{1}{\sin\Theta} \frac{\partial f}{\partial \Phi} \mathbf{e}_\Theta \right) \frac{r}{|\mathbf{r}-\mathbf{r}'|^3} V(\Theta,\Phi) \\ &= \frac{\mu_0 \sigma}{4\pi} \int d\Theta d\Phi \sin\Theta \, r \left\{ \frac{\partial f}{\partial \Theta} \left[\frac{r \sin\Theta' \sin(\Phi'-\Phi)}{|\mathbf{r}-\mathbf{r}'|^3} \right] \right. \\ &\quad \left. - \frac{1}{\sin\Theta} \frac{\partial f}{\partial \Phi} \left[\frac{r(\cos\Theta \sin\Theta' \cos(\Phi'-\Phi) - \cos\Theta' \sin\Theta)}{|\mathbf{r}-\mathbf{r}'|^3} \right] \right\} V(\Theta,\Phi). \end{aligned} \tag{10}$$

With the abbreviations $g = \sin\Theta \sin\Theta' \cos(\Phi'-\Phi) + \cos\Theta' \cos\Theta$ and

$$G = G(\mathbf{r},\mathbf{r}') = \frac{1}{|\mathbf{r}-\mathbf{r}'|} \tag{11}$$

we express the terms in curly brackets as

$$\frac{r \sin\Theta' \sin(\Phi'-\Phi)}{|\mathbf{r}-\mathbf{r}'|^3} = \frac{1}{r' \sin\Theta} \frac{\partial G}{\partial \Phi} + \frac{1}{r' \sin\Theta} \frac{r - r' g}{|\mathbf{r}-\mathbf{r}'|^3} \frac{\partial f}{\partial \Phi} \tag{12}$$

and

$$\begin{aligned} &\frac{r[\cos\Theta \sin\Theta' \cos(\Phi'-\Phi) - \cos\Theta' \sin\Theta]}{|\mathbf{r}-\mathbf{r}'|^3} \\ &\quad = \frac{1}{r'} \frac{\partial G}{\partial \Theta} + \frac{1}{r'} \frac{r - r' g}{|\mathbf{r}-\mathbf{r}'|^3} \frac{\partial f}{\partial \Theta}. \end{aligned} \tag{13}$$

Inserting this into Eq. (10) we finally arrive at the remarkably simple result

$$B_{r'} = \frac{\mu_0 \sigma}{4\pi r'} \int d\Theta d\Phi r \left(\frac{\partial G}{\partial \Phi} \frac{\partial f}{\partial \Theta} - \frac{\partial G}{\partial \Theta} \frac{\partial f}{\partial \Phi} \right) V + B_{r'}^{\inf}. \tag{14}$$

Note that if both the volume conductor and the source (and, hence, V) are axially symmetric (independent of Φ) we arrive after partial integration at the well known result that the magnetic field vanishes outside the volume conductor.

The crucial point is that there is no term of order $O(f^0)$ in Eq. (14), and hence, for a first order approximation we may set V to be the potential on the surface of a spherical volume conductor ($V \to V^0$) and evaluate G on the spherical surface ($G \to G^0$) resulting in

$$B_{r'} = \frac{\mu_0 \sigma R}{4\pi r'} \int d\Theta d\Phi \left(\frac{\partial G^0}{\partial \Phi} \frac{\partial f}{\partial \Theta} - \frac{\partial G^0}{\partial \Theta} \frac{\partial f}{\partial \Phi} \right) V^0 + O(f^2) + B_{r'}^{\inf}. \tag{15}$$

C. Explicit computation of the magnetic field

To explicitly evaluate the magnetic field for a dipolar source we express all functions in the integral kernel of Eq. (15) in series of spherical harmonics. While f is already formally given in Eq. (8) and G^0 is well known to be

$$G^0(\mathbf{r}',\mathbf{r}) = \frac{1}{|\mathbf{r}-\mathbf{r}'|} = \sum_{n=0}^{\infty} \sum_{m=-n}^{n} \frac{4\pi}{2n+1} \frac{R^n}{r'^{n+1}} \times \frac{Y_{n,m}^*(\Theta,\Phi) Y_{n,m}(\Theta',\Phi')}{N_{nm}^2} \tag{16}$$

with

$$\int d\Theta d\Phi \sin\Theta Y_{n,m}^*(\Theta,\Phi) Y_{n,m}(\Theta',\Phi') = \frac{4\pi}{2n+1} \frac{(n+|m|)!}{(n-|m|)!} =: N_{nm}^2 \tag{17}$$

we recall that for a unit charge monopole placed at $\mathbf{r}_0$ the potential on a spherical surface reads[19,23]

$$V_{\mathrm{mon}}^0(\mathbf{r},\mathbf{r}_0) = \frac{1}{\sigma} \sum_{k=1}^{\infty} \sum_{l=-k}^{k} \frac{1}{k} \frac{Y_{k,l}(\Theta,\Phi) Y_{k,l}^*(\Theta_0,\Phi_0)}{N_{kl}^2} \frac{r_0^k}{R^{k+1}}. \tag{18}$$

The potential for a current dipole with moment **J** can be found from Eq. (18) upon differentiation with respect to the origin.[19,24] This leads to

$$V^0_{\rm dip}(\Theta,\Phi)=\frac{1}{\sigma}\sum_{kl}\ \alpha_{kl}Y_{k,l}(\Theta,\Phi) \tag{19}$$

with

$$\alpha_{kl}=\mathbf{J}\nabla_0\frac{1}{k}\frac{r_0^k Y^*_{k,l}(\Theta_0,\Phi_0)}{R^{k+1}N_{kl}^2}, \tag{20}$$

where ∇_0 denotes the gradient with respect to $\mathbf{r}_0$.

Insertion of G^0, V^0, and f into Eq. (15) leads to a solution for the radial component of the magnetic field. Since **B** is curl free (in the quasistatic approximation) the complete magnetic field can be found from first calculating the scalar magnetic potential Φ and then taking its gradient

$$\mathbf{B}=\nabla\Phi=\nabla\int_\infty^r B_r\,. \tag{21}$$

After expanding B_r in a series of spherical harmonics integration along the radial direction is straightforward ending up with the final solution

$$\mathbf{B}(\mathbf{r}')=\frac{\mu_0}{4\pi}\sum_{n=1}^{N}\sum_{m=-n}^{n}\sum_{p=1}^{P}\sum_{q=-p}^{p}\sum_{k=1}^{N}\sum_{l=-k}^{k}\nabla'\times\frac{Y_{n,m}}{r'^{n+1}}\frac{R^{n+1}\beta_{pq}C_{nmpqkl}\alpha_{kl}}{(2n+1)(n+1)}+\mathbf{B}^{\rm sph}(\mathbf{r}') \tag{22}$$

with β_{pq} and α_{kl} defined in Eq. (8) and Eq. (20), respectively, and

$$C_{nmpqkl}\equiv\int_0^\pi d\Theta\int_0^{2\pi}d\Phi\,\frac{1}{N_{nm}^2}\times\left(\frac{\partial Y^*_{n,m}}{\partial\Theta}\frac{\partial Y_{p,q}}{\partial\Phi}-\frac{\partial Y^*_{n,m}}{\partial\Phi}\frac{\partial Y_{p,q}}{\partial\Theta}\right)Y_{k,l}, \tag{23}$$

where $\mathbf{B}^{\rm sph}$ denotes the solution for a spherical volume conductor. Here, we have already limited the sums to finite N and P as will be the case in a computer implementation. The proper choices will be discussed in the next section. Note, that the minus sign arising from integration of $1/r'^{n+2}$ in Eq. (21) has been put into the order of derivatives in Eq. (23).

At first sight it seems that evaluation of the sum in Eq. (23) over six indices is extremely time consuming, making it useless for practical applications. This is indeed not the case if, as in BEM, the computation is split into an initialization step which is independent of the source and a final step for each source.

For the initialization note that the C_{nmpqkl} in Eq. (23) are fixed numbers which need to be computed only once and can be stored (up to given order). Alternatively one may generate formulas (e.g., with Maple) which compute the nonvanishing elements for given p,q as a function of k and l. The latter is possible because the C_{nmpqkl} are sparse: the nonvanishing elements are constrained by

$$m=q+l \tag{24}$$

$$n=k+2j\quad\text{with}\quad -|p|+1\leqslant 2j\leqslant|p|-1. \tag{25}$$

The C_{nmpqkl} may be regarded as coupling constants between different spherical harmonics of the source V^0 and the solution **B**. For $p=0$ these couplings vanish; for $p=1$ the couplings correspond to a diagonal matrix, and for general p the ''coupling matrix'' has p side/main diagonals.

One very important consequence is that for finite p the convergence is controlled by r_0/r', the ratio of the sensor radius and the source radius, since, apart from constant factors, the radius of the unperturbed sphere R occurring in the factors $(R/r')^n$ in Eq. (22) and $(r_0/R)^k$ contained in the source coefficient α_{kl} cancels out. Now, in a practical application r_0/r' is always sufficiently smaller than 1: magnetic sensors cannot be put directly on the head surface and cortical current sources reside at least 15 mm below the skin-air boundary; hence, convergence will be excellent as is shown in the next section.

Coming back to the calculation of **B** the initialization consists of two steps.

(1) For the surface coefficients β_{pq} which parameterizes the perturbation around the sphere with radius R calculate

$$\tilde{C}_{nmkl}\equiv\frac{R^{n+1}}{(2n+1)(n+1)}\sum_{pq}\beta_{pq}C_{nmpqkl}\,. \tag{26}$$

(2) For each sensor at position $\mathbf{r}_i$ which measures **B** in direction $\mathbf{n}_i$ compute

$$\Psi^i_{nm}\equiv\frac{\mu_0}{4\pi}\mathbf{n}_i\nabla\frac{Y_{n,m}}{r_i^{n+1}} \tag{27}$$

and

$$\Phi^i_{kl}\equiv\sum_{nm}\ \Psi^i_{nm}\tilde{C}_{nmkl}\,. \tag{28}$$

The vectors Φ^i are the input for the explicit calculation of **B** for each source. We point out again that they have to be calculated only once for each volume conductor and sensor configuration. They correspond to the ''lead field'' of the ith sensor mapping the surface potential in the basis of spherical harmonics to the magnetic field.

Now, for the calculation of B_i, the magnetic field in the ith sensor, we have to compute α_{kl} according to Eq. (20) for each source and finally arrive at

$$B_i=\sum_{kl}\ \Phi^i_{kl}\alpha_{kl}+B_i^{\rm sph}. \tag{29}$$

Remarks: For notational simplicity we formulated the above algorithm using complex numbers. However, in practice one can save computation time if one splits the terms into real and imaginary parts and makes use of the fact that f, V^0 and G^0 are all real.

In the electric case we ended up with sums over a single index by making use of a coordinate transformation for each source rotating it to the z axis.[19] However, for large p this gets extremely complicated, and cannot be recommended. Furthermore, the convergence properties are far better for the magnetic case than for the electric case. The computation of the double sums is sufficiently fast, as shown in the next section.

The calculation of the magnetic field requires the evaluation of spherical harmonics and their derivatives. For the former we use standard algorithms,[25] and for the latter we

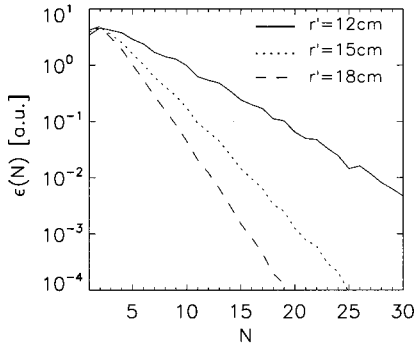

FIG. 1. Convergence: The relative difference between a magnetic field calculated up to order N of spherical harmonics and the same field calculated up to order 40 for a radial dipole placed on the surface ($z_0=9$ cm) of a spheroid, covered by a MEG whole head system of radius r'. The series converge exponentially as $\sim(z_0/r')^N$.

derived simple relations which reduce this problem to the former (see the Appendix).

III. PROPERTIES OF THE FORWARD CALCULATION

A. Convergence

The final perturbative solution for the magnetic field induced by a current dipole was given in Eq. (22) in terms of a sum of spherical harmonics. Practical applicability of this formula depends on its convergence behavior. Similar to the electric case the series converges exponentially with r_0/r' where r_0 is the radius of the source and r' is the radius of the measuring point. In contrast to the latter, magnetic sensors, being inside a dewar filled with liquid helium, cannot be placed directly on the skin. In practice this means that even for very superficial sources r_0/r' is rarely larger than 0.5, and one can expect the series to converge very fast.

Here, some care has to be taken since the ''matrix'' Eq. (23) contains off-diagonals extremely increasing the required number of terms. In general, for a surface parameterization with spherical harmonics up to order P corresponding to $(P+1)^2$ parameters a ''solution spherical harmonic'' of order n can couple (at most) to a ''source spherical harmonic'' of order $n\pm(P-1)$. Hence, the required order of the expansion of the solution may increase by $P-1$ compared to the naive expectation. At this point it is obvious that the sparseness of the coupling matrices in Eq. (26) is essential since otherwise the relevant expansion parameters would have been both r_0/R and R/r' with R being the radius of the unperturbed volume conductor.

In our computer implementation we go up to order $P=6$ corresponding to 49 parameters to describe the realistic volume conductor. In this case calculating the sum in Eq. (29) up to $N=20$ is sufficient as one can see in Fig. 1, where we plotted

$$\epsilon(N)\equiv\left\{\frac{\Sigma_i[B_i(40)-B_i(N)]^2}{\Sigma_i B_i^2(40)}\right\}^{1/2} \tag{30}$$

as a function of N, the order of spherical harmonics in Eq. (22). $B_i(N)$ denotes the perturbative magnetic field in the ith sensor calculated up to order N. As a sensor configuration we have chosen a virtual whole head system measuring the radial component of the magnetic field equally distributed around the whole volume conductor at radius r'. The source was defined to be a radial dipole placed on the z axis at height $r_0=9$ cm. The volume conductor corresponds to the prolate spheroid as used in the next section and the perturbative correction was calculated with respect to a sphere of radius $R=10$ cm. As one can see, for a measuring system with radius $r'=15$ cm corresponding to a source eccentricity of $r_0/r'=0.6$ the magnetic correction has converged for $N=20$ up to 0.1%. Indeed, the chosen sensor configuration has ''bad'' convergence properties: for a planar system at height $z'=12$ cm the ''error'' $\epsilon(N)$ is smaller than for the corresponding whole head system. Moreover, for a radial dipole individual terms in the series basically cancel: thus the considered case is exceptionally difficult.

For more accurate descriptions of the volume conductor corresponding to larger values of P a larger value of N is eventually needed. However, choosing, e.g., $N=30$ would still result in very fast forward calculations. Furthermore, the large spatial frequencies (large p) of the surface deformation have in general a small amplitude, and hence, for these coefficients a relatively less accurate forward calculation is sufficient.

B. Dependence on spatial frequencies

For the algorithm to compute the external magnetic field the order of spherical harmonics to parametrize the realistic surface is limited by an in principle arbitrary though finite number P. The larger P is chosen the higher is the computational cost. However, for a square integrable deformation f (any continuous deformation is square integrable) the sequence of surface coefficients, if written in the basis of normalized spherical harmonics, converges to zero. Moreover, for smooth deformations this convergence will be rapid.

Apart from this general considerations the question arises of how large is the impact of individual frequency components on the external field. In fact, if the surface potential is relatively smooth and the sensor configuration is not too close to the surface, contributions from higher order frequency surface deformations will basically cancel out, i.e., the mapping of the surface deformations to the magnetic field effectively acts as a spatial low pass filter.

To show this we have again used a spherical whole head system, as described in the last subsection, with radius r'. To the spherical volume conductor of radius $R=10$ cm we added ''pure'' normalized multipolar deformations

$$\beta_{pq}=\delta_{p_0p}\delta_{q_0q}N_{pq} \tag{31}$$

resulting in a correction to the magnetic field $B^i_{p_0q_0}$ in the ith sensor. Now for each order p_0 we calculated the mean

$$g(p_0)\equiv\frac{1}{2p_0+1}\sum_{q_0=-p_0}^{p_0}\left[\sum_i (B^i_{p_0q_0})^2\right]^{1/2}. \tag{32}$$

As a source we have chosen a radial dipole placed on the z-axis at height z_0. In Fig. 2 we show $g(p_0)$ for three values of r' and for various dipole depths. We see a clear exponen-

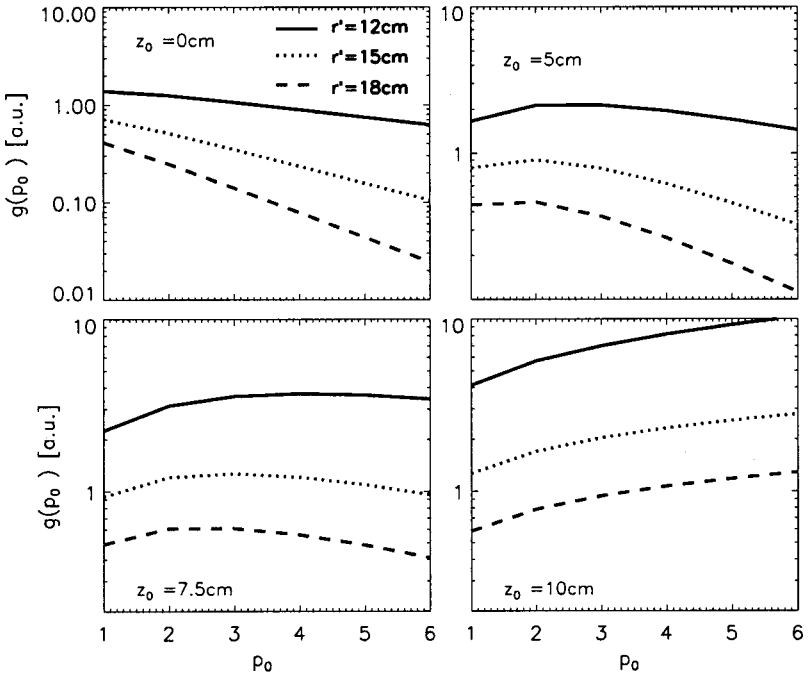

FIG. 2. The average contribution of different orders of the surface parameterization to the external magnetic field for whole head systems of radius r' and for various dipole locations (z_0).

tial decay of the norms of the magnetic fields. This exponential decay is the larger the farer the system is from the volume conductor. For more superficial sources this decay is less pronounced eventually resulting in an essentially constant $g(p_0)$ for sources placed on the surface of the volume conductor ($z_0 = R = 10$ cm).

In practice the distance from the dewar to the inner boundary of the skull is always large whereas the source can in general be quite close to this boundary. To conclude on this issue, the assumption of smoothness of the volume conductor is only necessary if superficial sources are considered: for deep sources high frequency oscillations of the volume conductor can always be neglected.

C. Computational cost

The computation of the magnetic field consists of three steps: (a) the parameterization of a given surface in a series of spherical harmonics, (b) the initialization for given surface parameters and sensor configuration, and (c) the actual calculation for each source. Computation times for each step are given for a HP 9000 (B180L) with 180 MHz.

To describe a surface by spherical harmonics we assume that it is given as a set of N_s points. Here, we first fit a sphere to these points which is a simple nonlinear fit with 4 parameters: the cost is proportional to N_s. Then we keep these parameters fixed and fit the deviation up to order P with $(P+1)^2$ parameters, which is a linear fit: the cost is proportional to $(P+1)^4 N_s$. Since the N_s points of the surface are in general not equally distributed as a function of surface angles we do not make use of the orthogonality of the spherical harmonics. For $P=6$ and $N_s=1600$, as was used for the prolate spheroid in the next section, this whole fit takes about 1.2 s. The splitting of the nonlinear sphere fit and the linear deviation fit speeds up (and simplifies) the calculation. However, we want to emphasize that this rather follows from the nature of perturbation theory: the unperturbed, spherical approximation should be as accurate as possible in order to obtain a small correction.

For the initialization we first construct the matrix $\tilde{C}$ according to Eq. (26). For each p,q and going up to order N both in the expansion of the source and the solution requires the calculation of $\sim pN^2$ matrix elements, and hence for $(P+1)^2$ different values of p,q the total cost increases as P^3N^2. For $N=20$ and $P=6$ this takes about 1 s. Now, for each sensor $\tilde{C}$ has to be applied on Ψ^i_{nm} [see Eq. (28)]. Since $\tilde{C}$ has $\sim P^2$ off-diagonals the total cost is proportional to $P^2N^2N_c$ with N_c being the number of channels. For $N_c=50$, $P=6$, and $N=20$ this takes about 1 s resulting in a total cost of 2 s for the initialization.

Finally, in addition to the spherical solution we have to construct α_{kl} according to Eq. (20) and calculate the ''scalar product'' with Φ^i_{kl} for each sensor to obtain the magnetic field [see Eq. (29)]. For $N_c=50$ channels a single forward calculation takes about 14 ms.

Both the initialization and the final computation of the magnetic field involve the evaluation of spherical harmonics *and* their derivatives. We would like to note that, with the help of the rules in the Appendix, the respective computational cost can be neglected.

The required disk space is considerably low because relatively small sparse matrices are involved. The coupling matrix $\tilde{C}$ in Eq. (26) has only $\sim P^2N^2$ nonvanishing elements and is constructed from $\sim P^3N^2$ nonvanishing fixed numbers C_{nmpqkl}. Additionally, the ''lead fields'' Φ^i_{kl} require the storage of $\sim N_cN^2$ numbers which is in general negligible.

IV. COMPARISON WITH THE PROLATE SPHEROID

As an illustrative example we will calculate the perturbative solution for the prolate spheroid, which roughly cor-

responds to the form of a realistic head volume conductor. We strongly emphasize again that the perturbation theory can be applied to arbitrary volume conductors as long as they are sufficiently smooth and as long as the deviation from a spherical fit is not too large. However, the spheroid is the only nonspherical volume conductor for which an exact solution exists, thus making it possible to evaluate the proposed approximate solution. Note, that the halfspace can be regarded as a special case of the spherical volume conductor.[3] Moreover, one cannot perturb around the halfspace within the proposed framework because the eccentricity of *any* source is 1.

The prolate spheroid is an egg-shaped surface defined by the image of the function

$$\mathbf{G}(\Theta,\Phi)=\begin{pmatrix} -\xi\cos\Theta \\ \sqrt{\xi^2-c^2}\sin\Theta\sin\Phi \\ \sqrt{\xi^2-c^2}\sin\Theta\cos\Phi \end{pmatrix}, \tag{33}$$

where ξ and c are fixed numbers. Here, we rotated the volume conductor as compared to the standard definition by 90° around the y axis in order to match the convention that the z coordinate corresponds to vertical direction.

Here we choose $\xi=12$ cm and $c=\sqrt{65}$ cm corresponding to $l=9$ cm (12 cm) for the short (long) half axis of the spheroid. These values roughly correspond to the typical distance ear to ear and front to back for a realistic case. This spheroid rather fits the skin than the inner skull of a typical head. However, relative errors do not depend on equal scale transformations of source, volume conductor, and sensor configuration. Moreover, the present choice is rather pessimistic in the sense that superficial sources have larger eccentricities than in typical real cases.

To use perturbation theory, the spheroid is approximated by a sphere plus a correction. This description is not unique. A reasonable choice is to use a fit both for the sphere and for the correction. However, it can be better to choose the sphere such that it approximates the realistic volume conductor in a region of interest: especially, for realistic cases, the sphere should rather fit the upper hemisphere if one is interested in cortical sources. Here, we discuss only two out of an infinite number of possibilities: (a) the sphere is chosen as a fit resulting in a radius of $R=10$ cm and (b) the sphere is defined to be the largest inner sphere having a radius of $R=9$ cm in order to be accurate on ''top'' of the volume conductor.

For both spheres the correction according to Eqs. (6) and (8) is defined as a least squares fit to $N_s=1600$ surface points. The spheroid and the two spheres are shown in Fig. 3. The spheres plus corrections up to order $P=6$ fit the spheroid with an accuracy of 99.99%: they are practically indistinguishable from the spheroid and are, hence, omitted in the figure. As measuring device we choose in this section a planar array of magnetometers at height $z=12$ cm. For definiteness, dipole moments are set to 20 nAm throughout this section.

To calculate the solutions of the prolate spheroid we use our arbitrary-precision implementation[26] of the Cuffin/Cohen series expansion.[10] The first 60 terms of the expansion were considered for the calculations. To make sure that 60 terms

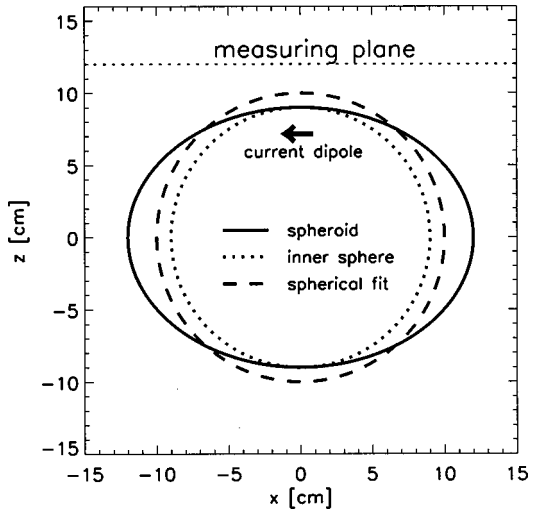

FIG. 3. The prolate spheroid and two spherical approximations. The approximation of the spheroid by spherical harmonics up to order $P=6$ is practically exact and not included in the figure. The dipole location and orientation are varied in the analysis — the plot shows a typical example.

are sufficient for a satisfying convergence, we compared the results to the results obtained with a considerable higher number of terms, namely 100. The relative differences of the solutions for 60 and 100 terms were less than 10^{-4} for all sources used in this article, which is sufficient to consider the solutions as ''exact'' for the comparisons to the different approximating solutions. The cutoff error is highest for the sources closest to the border of the volume conductor ($z_0=\pm 89$ mm) and decreases rapidly with increasing distance from the border, e.g., for $|z_0|\leqslant 80$ mm the relative cutoff error with 60 terms is only about 10^{-6}.

Let us first show two examples. In Fig. 4 we show the z components of the magnetic fields corresponding to a dipole placed on the z axis at height $z_0=4.5$ cm pointing into x direction. The perturbative solution was calculated with respect to the fitted sphere ($R=10$ cm). The spherical solution (upper, middle) deviates from the exact (upper, left) by 14% while the perturbative solution (upper, right) is 20 times more accurate having an error of only 0.7%. In the lower panel we show the respective difference fields. The perturbative correction (lower, middle) is in very good agreement to the ideal correction (lower, left), the exact field minus the spherical solution: the difference of the latter (lower, right) is about 20 times smaller than the ideal correction.

An interesting second example can be seen in Fig. 5. Here the dipole is located at $z_0=-1$ cm and points into y direction — the most difficult case for a nonsuperficial dipole. The perturbative solution was calculated with the inner sphere. While the spherical approximation breaks down completely, the perturbative solution correctly represents the complicated structure of the exact solution.

In the following we want to discuss in more detail the dependence of the accuracy of the forward calculations on the source parameters. We first restrict ourselves to the spherical and the perturbative solutions; the performance of BEM, which was also studied for comparison, will be discussed separately.

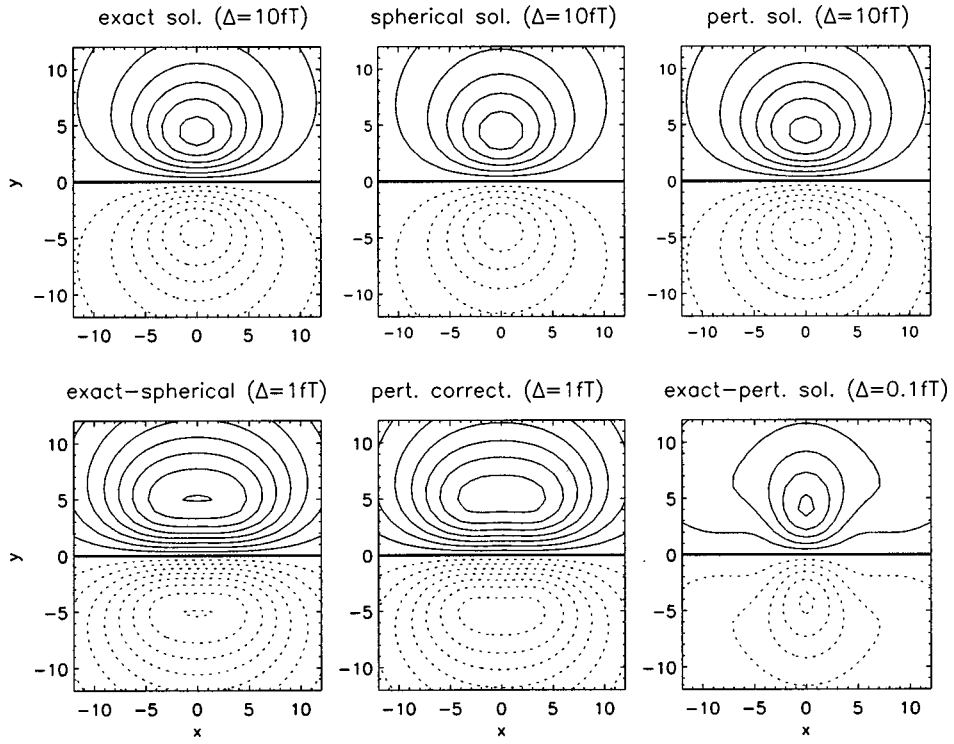

FIG. 4. Calcutated fields for a dipole located at $(x_0,y_0,z_0)=(0,0,4.5)$ cm pointing in x direction. Upper panel: exact solution (left), spherical approximation (middle), perturbative approximation (right). Lower panel: ideal correction to the sphere (left), calculated correction (middle), difference (ideal calculated) of the corrections (right).

In Fig. 6 this accuracy, defined as

$$\epsilon_\alpha=\left[\frac{\Sigma_i(B^i_{\text{exact}}-B^i_{\text{approx}})^2}{\Sigma_i(B^i_{\text{exact}})^2}\right]^{1/2}, \tag{34}$$

where $\alpha=x,y,z$ denotes the measured component of the magnetic field, is shown as a function of dipole depth z_0. The accuracy was calculated for the spherical approximation and for the perturbative solutions with respect to a fitted sphere of radius $R=10$ cm (''pert. a)'' and to an inner sphere of radius $R=9$ cm (''pert. b).'' Apart from the central dipole pointing in z direction the inner sphere works better than the fitted sphere. Especially, if a ''radial'' dipole approaches the surface at $z_0=9$ cm the fitted sphere may result in large relative errors. The reason for this is that the exact solution

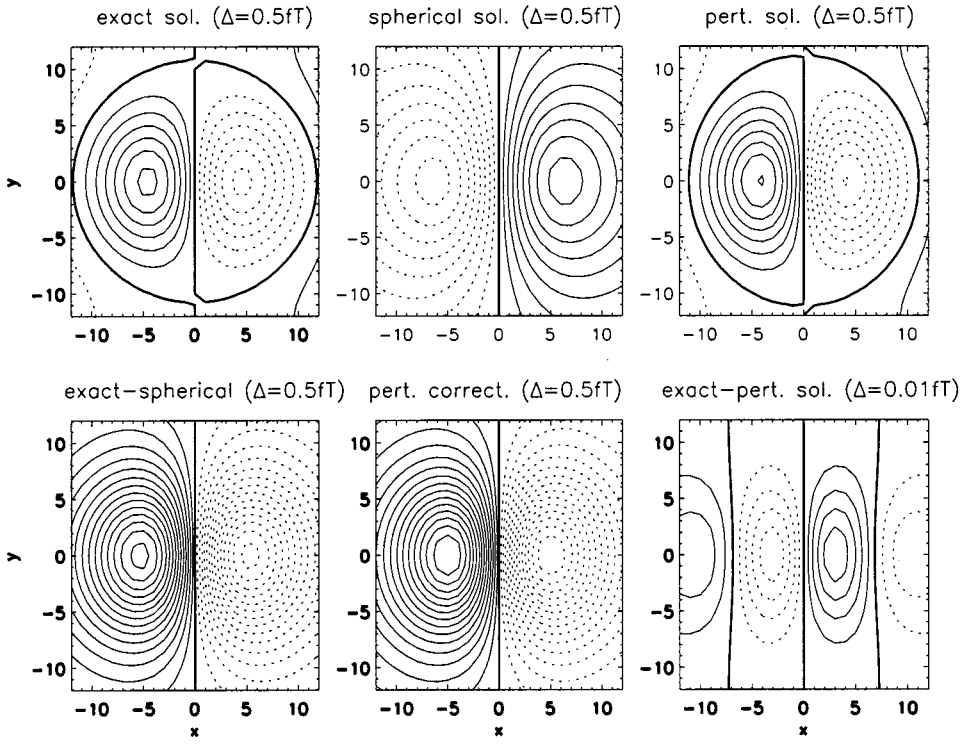

FIG. 5. Same as Fig. 4 for a dipole located at $(x_0,y_0,z_0)=(0,0,-1)$ cm pointing in y direction.

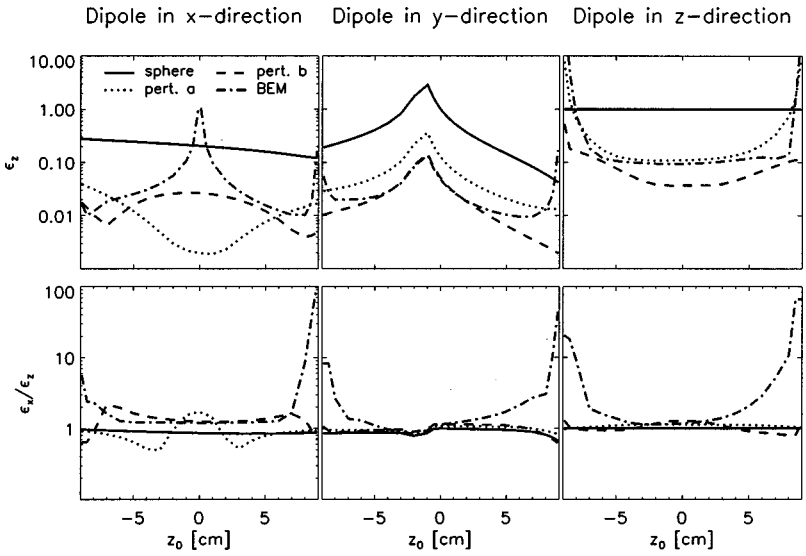

FIG. 6. Upper panel: Error of the forward calculation for various approximations of the forward calculation as a function of dipole height for the *z* component of the magnetic field. Lower panel: Ratio of the corresponding error of the *x* component and the *z* component. The terms pert. a and pert. b refer to the perturbative expansions around a sphere of radius $R=10$ cm and $R=9$ cm, respectively.

converges to zero in this limit: if the perturbative solution is calculated with a sphere of correct radius (at the considered location) it has this same property and hence the error stays finite. However, also for other dipole directions the inner sphere is more appropriate for superficial sources as was the purpose of this very choice.

In the center of the volume conductor the relative error eventually increases as can be seen for a dipole pointing in *y* direction. The basic reason is that tangential dipoles get more radial when approaching the center and, hence, the exact solution decreases. Remarkably, this increase cannot be seen for the dipole in *x* direction: the exact and the perturbative solution converge to zero due to axial symmetry resulting in a finite error. We note, that for this case the point at $z_0=0$ was excluded in the figure since for the accuracy one divides zero by zero.

Quite generally, perturbation theory improves the spherical approximation by about a factor 10–20 with exceptional cases in both directions: while one should be careful with radial dipoles approaching the surface, the improvement due to perturbative corrections can be much more dramatic for intermediate dipoles eventually giving rise to an error decrease by a factor 100.

Finally, we want to compare the results for the analytical approximation with the corresponding numerical solution given by BEM using the program ''Curry'' (Philips). For the latter we used a surface parameterization consisting of 2610 triangles with a typical side length of about 8 mm. In fact, we used a given liquor triangularization and transformed the triangles and normals to parametrize the spheroid.

As can be seen from Fig. 6 the relative accuracy of BEM depends very much on the location and the direction of the dipole. Generally, BEM becomes poor in the vicinity of the surface of the volume conductor: for the *z* component of the magnetic field this increase of the error starts at about 1 cm distance ($\approx$ triangle length) from the surface and becomes unacceptable at half the triangle length in agreement with other findings.[12]

BEM works satisfactory for nonsuperficial sources apart from the case of a central dipole pointing in *x* direction. However, this extreme breakdown of performance is basically caused by the vanishing of the true solution. Perturbation theory based on the inner sphere works always better than BEM while the corresponding solution for the fitted sphere is eventually worse in regions of good performance of BEM.

The breakdown of BEM in the vicinity of the surface is more pronounced if a nonvertical field component is studied. From the lower panel of Fig. 6 it can be seen that analytical solutions, being exactly curl-free, behave similar for all field components. In contrast, a large increase of the error of BEM is observed at the boundaries: the contribution of the volume current arises from relatively few, basically vertical secondary currents (i.e., triangles) which induce a basically nonvertical magnetic field. If the *x* component of the magnetic field is studied then also the ''bad'' perturbative solution (fitted sphere) has always smaller errors than BEM for sources closer than 3 cm to the surface, and even the spherical solution is better than BEM for sources closer than 1 cm.

V. CONCLUSION

We presented the theory to compute an analytical approximation of the external magnetic field due to a source inside a realistic volume conductor. We assumed that the volume conductor can be described by a sphere plus a small correction. It was shown that a first order Taylor expansion of the magnetic field with respect to this correction can be given without referring to the corresponding electric solution. The central result of the proposed theory, given in Eq. (14), is a remarkably simple integral for the calculation of the radial component of the magnetic field, from which all other components follow resulting in an exactly curl-free approximation.

An explicit computer implementation of the theory can only be done for a finite parameterization of the realistic volume conductor. Then, perturbation theory leads to a coupling of input, the surface potential calculated in the spherical approximation, and output, the magnetic field at some specific location, consisting of a sparse and diagonally domi-

nant matrix. The latter property ensures that the final solution, which is written as a series of spherical harmonics, converges as $\sim(r_0/r')^n$ where r_0 (r') denotes the radial coordinate of the source (sensor). In practice, even for superficial sources r_0/r' is substantially smaller than 1 resulting in very fast algorithms for both the initialization and the actual forward calculation.

We presented a detailed analysis of the performance of the proposed approximation by comparing it to the analytical solution for a (prolate) spheroid, the only nontrivial volume conductor where an exact solution is known. With the long axis being 33% larger than the two short axes the assumed deformation of the sphere is rather an overestimate of realistic deformations. Quite generally we found that the perturbative solution improves the spherical approximation by a factor 10–20 with exceptions in both directions. Especially we found no problems with very superficial tangential sources; radial sources eventually show up a diverging *relative* error because the exact solution vanishes for sources placed on the surface giving rise to an intrinsically singular performance measure.

For comparison we also calculated the corresponding BEM solutions. We found BEM to be satisfactory for deep sources with an error being in the same order as the perturbative approach. Details, however, depend on the dipole direction and the location and on the specific realization of the perturbative approximation. BEM eventually breaks down for superficial sources. While the corresponding increase of the error occurs only for sources very close to the surface (≈ 5 mm) if an essentially radial (here: vertical) component of the magnetic field is studied, the tangential (here: horizontal) field components show a breakdown of the performance much earlier (≈ 2 cm). This is in sharp contrast to analytical methods which lead to exactly curl-free solutions.

We demonstrated the performance of a first order perturbation theory for a single surface parametrized by 49 parameters. Generalizations can be done with respect to all aspects: especially in conjunction with the corresponding electric solution[19] the theoretical basis is given, and the computational cost, being so far extremely low, can be expected to be within acceptable limits.

ACKNOWLEDGMENTS

Supported by DFG Ma 1782/3. The authors would like to extend our appreciations to Samual J. Williamson and Jan C. de Munck for helpful discussions.

APPENDIX

Here, we present some very useful relations to calculate derivatives of spherical harmonics, which are not known so far. Phase and normalization conventions are as in Ref. 19. Let us define

$$F_{n,m}(\mathbf{r}) \equiv r^n Y_{n,m}(\Theta,\Phi) \tag{A1}$$

then from standard recursion relations it follows that

$$\left(\frac{\partial}{\partial x} + i\frac{\partial}{\partial y}\right) F_{n,m} = -F_{n-1,m+1} \quad \forall m \geqslant 0, \tag{A2}$$

$$\left(\frac{\partial}{\partial x} - i\frac{\partial}{\partial y}\right) F_{n,m} = (n+m-1)(n+m) F_{n-1,m-1} \quad \forall m > 0, \tag{A3}$$

$$\frac{\partial}{\partial z} F_{n,m} = (n+m) F_{n-1,m} \quad \forall m \geqslant 0. \tag{A4}$$

The corresponding rules for $m<0$ in Eq. (A2) follow from complex conjugation of Eq. (A3) and similarly for the other rules. Calculation of ∇F_{nm} corresponds to simple combinations of Eqs. (A2)–(A4). Here, we have to calculate the gradients of $r^n Y_{n,m}$ and $Y_{n,m}/r^{n+1}$. The latter can be calculated from Eqs. (A2)–(A4) by writing $Y_{n,m}/r^{n+1} = F_{n,m}/r^{2n+1}$.

[1] M. S. Hämäläinen, R. Hari, R. J. Ilmoniemi, J. Knuutila, and O. V. Lounasma, Rev. Mod. Phys. **65**, 413 (1993).
[2] E. Frank, J. Appl. Phys. **23**, 1225 (1952).
[3] J. Sarvas, Phys. Med. Biol. **32**, 11 (1987).
[4] J. C. de Munck and M. J. Peters, IEEE Trans. Biomed. Eng. **40**, 1166 (1993).
[5] D. A. Brody, F. H. Terry, and R. E. Ideker, IEEE Trans. Biomed. Eng. **20**, 141 (1973).
[6] P. M. Berry, Ann. N.Y. Acad. Sci. **65**, 1126 (1956).
[7] J. C. de Munck, J. Appl. Phys. **64**, 464 (1988).
[8] P. Lambin and J. Troquet, J. Appl. Phys. **54**, 4174 (1983).
[9] A. S. Ferguson and G. Stroink, J. Appl. Phys. **76**, 7671 (1994).
[10] B. N. Cuffin and D. Cohen, IEEE Trans. Biomed. Eng. **24**, 372 (1977).
[11] M. Rosenfeld, R. Tanami, and S. Abboud, IEEE Trans. Biomed. Eng. **43**, 679 (1996).
[12] J. C. de Munck, IEEE Trans. Biomed. Eng. **39**, 986 (1992).
[13] A. S. Ferguson, X. Zhang, and G. Stroink, IEEE Trans. Biomed. Eng. **41**, 445 (1994).
[14] M. Fuchs, R. Drenckhahn, H.-A. Wischmann, and M. Wagner, IEEE Trans. Biomed. Eng. **45**, 980 (1998).
[15] G. Nolte and G. Curio, Biophys. J. **73**, 1253 (1997).
[16] T. F. Oostendorp and A. van Oosterom, IEEE Trans. Biomed. Eng. **43**, 394 (1996).
[17] Y. Wang, IEEE Trans. Biomed. Eng. **45**, 131 (1998).
[18] G. Nolte and G. Curio, IEEE Trans. Biomed. Eng. **46**, 400 (1999).
[19] G. Nolte and G. Curio, J. Appl. Phys. **86**, 2800 (1999).
[20] C. Purcell, T. Mashiko, K. Okada, and K. Ueno, IEEE Trans. Biomed. Eng. **38**, 303 (1991).
[21] M. X. Huang, J. C. Mosher, and R. M. Leahy, Phys. Med. Biol. **44**, 423 (1999).
[22] M. S. Hämäläinen and J. Sarvas, IEEE Trans. Biomed. Eng. **36**, 165 (1989).
[23] Z. Zhang and D. L. Jewett, Electroencephalogr. Clin. Neurophysiol. **88**, 1 (1993).
[24] A. S. Ferguson and D. Durand, J. Appl. Phys. **71**, 3107 (1992).
[25] W. H. Press, S. A. Teukolsky, W. T. Vetterling, and B. P. Flannery, *Numerical Recipes in C* (Cambridge University Press, Cambridge, 1992).
[26] T. Fieseler, *Analytic Source and Volume Conductor Models for Biomagnetic Fields* (Shaker, Aachen, Germany, 2000).